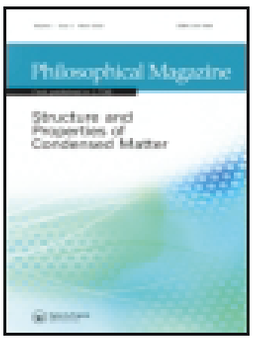

Philosophical Magazine

ISSN: 1478-6435 (Print) 1478-6443 (Online) Journal homepage: https://www.tandfonline.com/loi/tphm20

An investigation of the stored energy and thermal stability in a Cu–Ni–Si alloy processed by high-pressure torsion

Hiba Azzeddine, Yousf Islem Bourezg, Abdel Yazid Khereddine, Thierry Baudin, Anne-Laure Helbert, François Brisset, Megumi Kawasaki, Djamel Bradai & Terence G. Langdon

To cite this article: Hiba Azzeddine, Yousf Islem Bourezg, Abdel Yazid Khereddine, Thierry Baudin, Anne-Laure Helbert, François Brisset, Megumi Kawasaki, Djamel Bradai & Terence G. Langdon (2019): An investigation of the stored energy and thermal stability in a Cu–Ni–Si alloy processed by high-pressure torsion, Philosophical Magazine

To link to this article: https://doi.org/10.1080/14786435.2019.1703055

Published online: 20 Dec 2019.

PHILOSOPHICAL MAGAZINE
https://doi.org/10.1080/14786435.2019.1703055

Taylor & Francis
Taylor & Francis Group

An investigation of the stored energy and thermal stability in a Cu–Ni–Si alloy processed by high-pressure torsion

Hiba Azzeddine[a], Yousf Islem Bourezg[b,c], Abdel Yazid Khereddine[d], Thierry Baudin[e], Anne-Laure Helbert[e], François Brisset[e], Megumi Kawasaki [f], Djamel Bradai[b] and Terence G. Langdon [g]

[a]Faculty of Technology, University of Mohamed Boudiaf, M'sila, Algeria; [b]Faculty of Physics, University of Sciences and Technology Houari Boumediene, Algiers, Algeria; [c]Department of Physics, University Ziane Achour of Djelfa, Djelfa, Algeria; [d]Centre de Développement des Technologies Avancées, CDTA, Algiers, Algeria; [e]ICMMO, Univ. Paris-Sud, Université Paris-Saclay, Orsay Cedex, France; [f]School of Mechanical, Industrial and Manufacturing Engineering, Oregon State University, Corvallis, OR, USA; [g]Materials Research Group, Department of Mechanical Engineering, University of Southampton, Southampton, UK

ABSTRACT

The stored energy and activation energy for recrystallization were investigated for a Cu-Ni-Si alloy after high-pressure torsion processing for $N = ½$, 1, 5 and 10 turns at room temperature. The contributions of geometrically necessary dislocations (GNDs), statistically stored dislocations (SSDs) and vacancies to the stored energy were calculated through the Vickers microhardness measurements, kernel average misorientation (KAM) measurements and an analysis by differential scanning calorimetry (DSC). The results show that the total stored energy decreases rapidly after equivalent strain of $\varepsilon_{eq} \sim 9$ and then saturates through $\varepsilon_{eq} \sim 86$ at ~70 J/mol. Concurrently, the local stored energy in GNDs and SSDs was found to depend strongly on the radial distance from the centre of the disc and increase with increasing equivalent strain at $\varepsilon_{eq} \sim 16$ and saturate with further straining. Accordingly, the results indicate that the GNDs and vacancies are responsible for the high stored energy in the initial stage of deformation at equivalent strain range of $\varepsilon_{eq} = 8.6–16$ and thereafter their contribution decreases slightly due to the occurrence of dynamic recrystallization and the formation of fine grains. At the same time, the contribution of the SSDs is similar to that of the GNDs only in high strain deformation as at $\varepsilon_{eq} = 49.3$ to accommodate the deformation process. An activation energy for recrystallization was estimated in the range of ~89.7–98.7 kJ/mol, thereby suggesting poor thermal stability.

ARTICLE HISTORY
Received 15 June 2019
Accepted 6 December 2019

KEYWORDS
Copper alloy; DSC; hardness; recrystallization; severe plastic deformation; stored energy

CONTACT Hiba Azzeddine hiba.azzeddine@univ-msila.dz; azehibou@yahoo.fr Faculty of Technology, University of Mohamed Boudiaf, M'sila, Algeria

1. Introduction

During the last decades, processing using severe plastic deformation (SPD), including equal-channel angular pressing (ECAP) and high-pressure torsion (HPT), has been successfully developed to produce bulk ultrafine-grained (UFG) materials [1,2]. The combination of a very small grain size and a defect structure introduced during processing leads to a high yield strength and additional excellent mechanical properties in the copper-based alloys [3–7]. In practice, processing by ECAP is extensively used and well investigated due to the beneficial ability to process large bars and billets which have a high potential for subsequent structural applications in industry [1]. Nevertheless, processing by HPT is recognised to produce exceptional grain refinement and to produce a stabilised microstructure having a high fraction of high-angle grain boundaries (HAGBs) [8,9].

It is well known that the stored energy in deformed microstructures, mostly in the form of dislocation substructures and high concentrations of vacancies, plays a significant role in controlling the nucleation of recrystallization and this will affect the mechanical anisotropy of the materials [10,11]. An estimate of the stored energy may be undertaken using several different techniques. For example, the total stored energy can be measured by differential scanning calorimetry (DSC) [12] and the local stored energy can be estimated from microhardness measurements [13], diffraction line broadening analysis by X-rays [14] and neutron diffraction [15] or by electron back-scatter diffraction (EBSD) [16].

Accordingly, numerous investigations were reported describing the stored energy and thermal stability of copper-based alloys processed by ECAP [4,10,11,17–20] and it was found that the stored energy increases with increasing ECAP processing up to 12 passes (~50 J/mol) and thereafter decreases gradually between 16 and 24 passes [21]. Moreover, ECAP processing tends to show a higher stored energy and a lower activation energy in copper compared with the values obtained after cold rolling [10]. It was reported that annealing at low-temperature (100–300°C) can improve the mechanical properties of HPT copper alloy by increasing the electro-conductivity and decreasing the wear rate [22]. However, the copper alloys processed by HPT suffer from low thermal stability [23–26]. The recrystallization peak was detected at 220°C with an activation energy of 94.5 kJ/mol for the present purity of Cu (98.5%) after 1 HPT turn using DSC analysis [27]. A similar recrystallization temperature (190°C) was reported in highly pure Cu (99.99%) processed by HPT using positron lifetime annihilation spectroscopy measurements [28].

There are many reports on the self-annealing at room temperature in processed copper by HPT [29–31]. Recently, it was shown that there was a very significant self-annealing effect after room temperature storage for 6 weeks in high

purity Cu processed by HPT after $N = ½$ turn whereas the effect was absent after $N = 5$ and 10 turns [29]. Nevertheless, studies devoted to analysing the stored energy and activation energy of recrystallization of HPT-processed copper alloys are limited. Thus, the aim of the present research was to evaluate the stored energy in a commercial Cu–Ni–Si alloy after HPT processing at room temperature through 10 turns. First, the evolution of the total stored energy was investigated by DSC measurements. Second, the local stored energy was measured by microhardness testing and a kernel average misorientation (KAM) approach using an EBSD technique in order to quantify the contributions of the different defect sources to the total stored energy. The evolution of the activation energy of recrystallization was also examined in order to investigate the thermal stability of the Cu–Ni–Si alloy.

2. Experimental material and procedures

A commercial Cu–2.5Ni–0.6Si (wt.%) plate alloy with dimensions of $160 \times 102 \times 11$ mm^3 was supplied by CLAL-MSX (Meru, FRANCE) as a supersaturated solid solution after hot rolling at 820°C and quenching in water. Discs with a thickness of 0.8 mm and a diameter of 10 mm were machined from the plate and then processed by HPT for $N = ½$, 1, 5 and 10 revolutions at room temperature using an imposed pressure of 6.0 GPa and a rotational speed of 1 rpm. The HPT processing was performed under quasi-constrained conditions where there is a small outflow of material around the edge of the disc between the two anvils [32].

It is well establish that the strain distribution within an HPT-processed disc is inhomogeneous and depends on the radial distance from the centre of the disc according to the expression [2]:

$$\varepsilon_{eq} = \frac{\gamma}{\sqrt{3}} = \frac{2\pi N r}{h\sqrt{3}} \tag{1}$$

where γ, N, r and h are the shear strain, the number of HPT turns, the radial distance from the centre of the disc and the thickness of the disc, respectively. It was reported that the final thickness of the sample depends slightly on the number of HPT turns [33]. However, in the absence of any thickness measurements, the present calculations assume a constant thickness of $h = 0.85$ mm.

2.1. Electron backscatter diffraction (EBSD)

The EBSD measurements were performed in the RD-SD plane of the processed discs where RD and SD denote the rotational and shear directions, respectively. The microstructures were investigated near the centre at $r = 0.4$ mm and near the edge at $r = 4.5$ mm of the deformed discs using a scanning electron

microscope FEG-SEM SUPRA 55 VP operating at 20 kV. The EBSD data acquisition and analysis were undertaken using TSL Orientation Imaging Microscopy, OIM^{TM} software.

The scanned areas were 100×100 μm^2 with a step size of 0.1 μm for the disc processed through $N = ½$ turn and 25×25 μm^2 with a 25 nm step size for the remainder of the processed discs after $N = 1$, 5 and 10 turns. The grain size data were obtained using a grain tolerance angle of 5° and the minimum grain size was chosen as 2 pixels.

The confidence index (CI) quantifies the reliability of the indexed Kikuchi pattern and only datum points with CI higher than 0.05 (indexing reliability is 95%) were taken into account to exclude poor quality pixels and to avoid possible errors introduced during the cleanup procedures [34]. The data taken from each sample included more than 2000 grains.

A quantification of the recrystallization processes for the HPT-deformed samples was estimated by applying the Grain Orientation Spread (GOS) criterion where GOS is the average deviation between the orientation of each point in the grain and the average orientation of the grain [35], where the recrystallized grains are separated from the deformed grains with values of GOS <1° [35].

Generally, KAM is used to quantify the average misorientation between a given point and its nearest neighbours which belong to the same grain [36] where KAM reflects the distribution of strain and the dislocation density on individual measurement points [37]. The misorientation angle, θ_{KAM}, is connected directly with the plastic strain stored energy as well as the density of geometrically necessary dislocations, ρ [38,39]:

$$\rho = \frac{\alpha \theta_{KAM}}{ndb} \tag{2}$$

where α is a parameter which depends on the grain boundary type with values of 2 and 4 for pure tilt and twist boundaries, respectively [40], $b = 0.255$ nm is the Burgers vector, n is for the nearest neighbour and d is the EBSD scan step size. The θ_{KAM} value was calculated from the mean misorientation angle between the point and its three neighbours excluding misorientations greater than 5°.

It is well known that the magnitude of the KAM value is affected by the scan step size [40–42]. The difference of the chosen scan step size for the disc after $N = ½$ turn and the other processed discs was unintentional. Thus, it is reasonable to use the normalised KAM value (θ_{KAM}/d) to directly compare the evolution of the KAM value as a function of the numbers of HPT turns.

It is known that the KAM value depends on the EBSD clean-up parameters (grain tolerance angle and minimum grain size). In this case, a measurement of KAM values was also performed using a grain tolerance angle of 3° and the

minimum grain size of 2 pixels. The difference between the two clean-up procedure was found to be very small, $\Delta\theta_{KAM} = 0.05°$.

Subsequently, the stored energy from the estimated dislocation density was estimated using the following equation [38,39]:

$$E_{KAM} = \frac{1}{2}\rho\mu b^2 = \frac{\mu b \theta_{KAM}}{2d} \tag{3}$$

where μ is the shear modulus having a value of $\mu = 48.3$ GPa for copper.

2.2. Vickers microhardness

The Vickers microhardness, Hv, was measured using a Zwick 3212 microhardness tester near the centres ($r = 0.4$ mm) and edges ($r = 4.5$ mm) of the deformed samples with a load of 0.98 N maintained for 10 s. The average hardness at each position were estimated from four individual points recorded around the selected position and separated by distances of 0.15 mm. It is noted that using four points is a standard procedure for measuring Hv and the highest error for the Hv measurements was estimated to be about 5%.

The dislocation density was estimated from the H_V values using the Taylor equation [13,43]:

$$\rho = \frac{1}{13.5}\left(\frac{H_v - H_{v0}}{M\alpha\mu b}\right)^2 \tag{4}$$

where $H_{V0} = 82.12$ is the microhardness of the initial sample prior to deformation [8], M is the Taylor factor of ~3.08 and $\alpha = 0.22$ is a constant. Hence, the stored energy, E_{Hv}, may be obtained from the Hv values using the following equation [13]:

$$E_{Hv} = \frac{1}{2}\rho\mu b^2 = \frac{1}{27\mu}\left(\frac{H_v - H_{v0}}{M\alpha}\right)^2 \tag{5}$$

2.3. Differential scanning calorimetry (DSC)

The total stored energy and activation energy for recrystallization of the deformed samples were calculated by DSC analysis. Samples with weights of 45−50 mg were cut near the centres of the discs and then inserted in an aluminum crucible having a diameter of 5 mm and subjected to DSC analysis using a 2920 MDSC calorimeter under a nitrogen atmosphere. Data obtained with an empty Al crucible was used as a reference. The DSC experiments were performed using four heating rates of 10°C/min, 20°C/min, 30°C/min and 40°C/min and with scanning temperature ranging from 80°C to 500°C. The total stored energy, E_{DSC}, of the deformed samples was estimated based on the area

of the heat release from the recrystallization peak [12]. However, it is useful to mention that in future investigations it will be better to extend the temperature range even lower to room temperature especially with a high heating rate such as 40°C/min in order to obtain more accurate measurements.

The activation energy for recrystallization was calculated using the dependence of the peak temperature on the heating rate (10°C/min, 20°C/min, 30°C/min and 40°C/min) given by the Boswell method [44,45]:

$$\ln\left(\frac{V}{T_p}\right) = C - \frac{E}{RT_p} \tag{6}$$

where V is the heating rate, E is the activation energy, T_p is the maximum temperature at the peak, R is the universal gas constant and C is a constant. From a statistical viewpoint, it important to note that only one sample was used for each method to estimate the stored energy.

3. Results

3.1. Stored energy estimates

Figure 1 presents a compilation of the DSC scans at four different heating rates of 10°C/min, 20°C/min, 30°C/min and 40°C/min demonstrating the

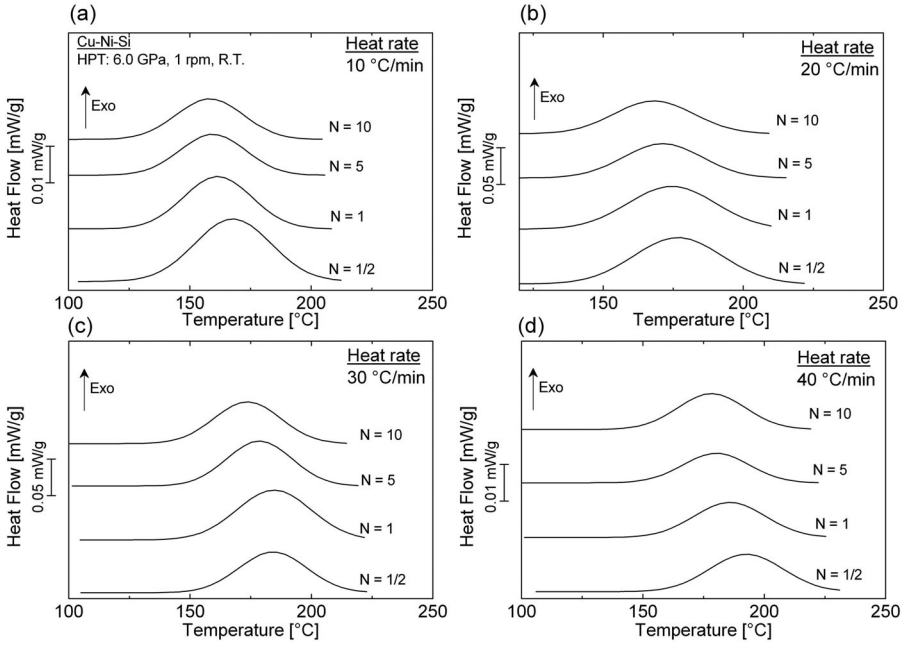

Figure 1. DSC scans at a heating rate of 10°C/min, 20°C/min, 30°C/min and 40°C/min corresponding to the recrystallization phenomena in Cu–Ni–Si alloy processed by HPT for $N = ½$, 1, 5 and 10 turns respectively.

recrystallization peaks for the Cu–Ni–Si alloy processed by HPT through $N = ½$, 1, 5 and 10 turns. It is worth noting that the DSC curves over the full range (80–500°C) contain several exothermic and endothermic peaks belonging to a complex sequence of precipitation. For the purpose of this report, only the first exothermic peak corresponding to the recrystallization phenomenon is considered. It is reasonable to mention also that no recovery peak before the recrystallization peak was detected in the DSC curves. Previously, it was shown that no precipitation was detected in the Cu–Ni–Si alloy during HPT processing [46]. Moreover, the quasi-binary section of the ternary Cu–Ni–Si phase diagram and recent results on the precipitation kinetics of the same Cu–Ni–Si alloy after HPT processing indicate that the precipitation of the δ-Ni_2Si and γ-Ni_5Si_2 phases occur at high annealing temperatures ranging from 450°C to 700°C [46]. It is apparent that the discs processed by higher numbers of HPT turns show peaks at lower recrystallization temperatures at each heating rate. Moreover, a significant peak shift towards a higher temperature is observed upon increasing the heating rate. Nevertheless, the DSC scans exhibit peaks extending more or less between 120°C and 220°C for all measurement conditions. For better visualisation of Figure 1, the results are re-plotted in Figure 2 as the peak recrystallization temperature against the equivalent strain at each heating rate for the Cu–Ni–Si alloy. It is to be noted that the equivalent strain, $\varepsilon_{eq,}$ for the DSC measurement was taken as the mean value between the centre and the edge of the HPT discs. This plot shows a trend that the temperature peak of recrystallization first decreases with increasing equivalent strain to $\varepsilon_{eq} \sim 49.3$ ($N = 5$ turns) and then tends to stabilise where the temperature peak of recrystallization remains unchanged with further straining.

Figure 3 presents the KAM maps corresponding to the 1st neighbour with 5° threshold angle and GOS maps near the centres (left column) and edges (right column) of the discs processed by HPT for $N = ½$, 1, 5 and 10 turns, respectively.

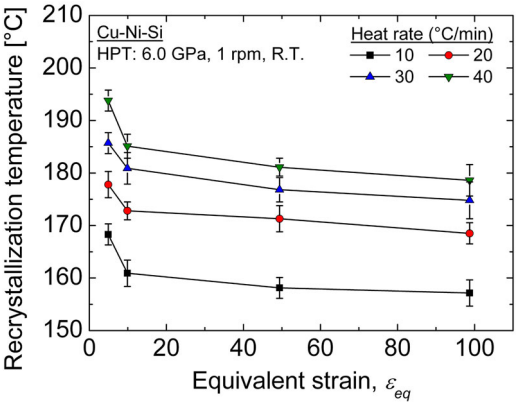

Figure 2. Evolution of the recrystallization temperature peak of Cu–Ni–Si alloy as function of equivalent strain.

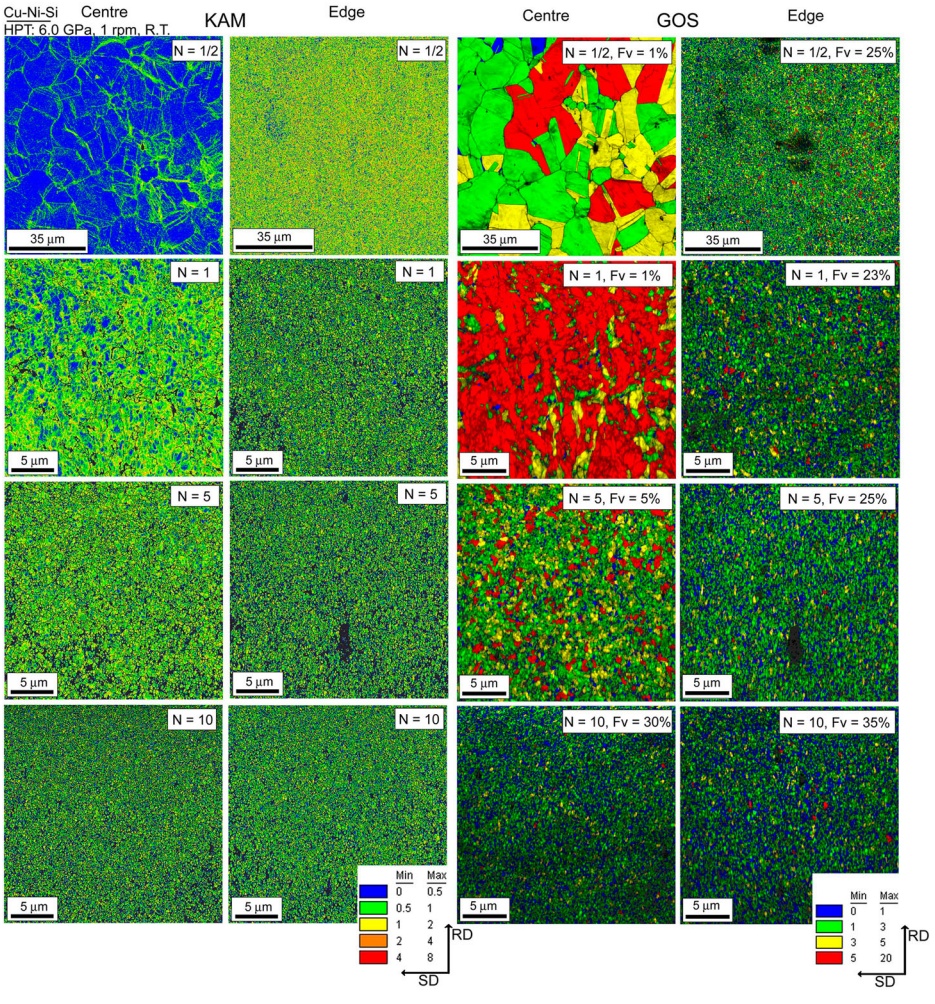

Figure 3. KAM and GOS maps near the centre (left column) and near the edge (right column) of Cu–Ni–Si discs processed by HPT for $N = ½$, 1, 5 and 10 turns, respectively.

The estimated volume fractions of recrystallization, *Fv*, are specified in each GOS map. Significant microstructural refinement is apparent at the edges from the early stage of HPT from $\varepsilon_{eq} = 8$ ($N = ½$ turn) through $\varepsilon_{eq} = 160$ ($N =$ 10 turns) and there is a gradual refinement at the disc centres followed by a reasonable level of homogeneity along the disc diameter after $\varepsilon_{eq} = 16$ ($N = 10$ turns). More details on the evolution of microstructural parameters such as grain size, grain boundary distributions and crystallographic texture of the same Cu–Ni–Si alloy after HPT processing was reported earlier [5]. Figure 3 shows that after $N = ½$ and 1 turn, the disc centre showed severe grain refinement but with low *Fv* of ~1% but the *Fv* value increased to ~ 25% at the edge of the discs for both $N = ½$ ($\varepsilon_{eq} = 8$) and 1 turns ($\varepsilon_{eq} = 16$). The microstructure after $N = 5$ turn ($\varepsilon_{eq} = 80$) maintains microstructural heterogeneity between

these regions but it is apparent that the microstructure after $N = 10$ turns ($\varepsilon_{eq} = 160$) achieved reasonable homogeneity and contained about ~30–35% of recrystallized grains in both the disc centre and edge.

The evolution of the normalised KAM value (θ_{KAM}/d) as a function of the numbers of HPT turns is shown in Figure 4(a). The KAM values near the centres of the Cu–Ni–Si alloy discs increase from 5 to 40°/μm with increasing HPT turns from $N = ½$ turn ($\varepsilon_{eq} = 0.8$) to $N = 5$ turns ($\varepsilon_{eq} = 8$) and this is followed by a decrease to 35.5°/μm after $N = 10$ turns ($\varepsilon_{eq} = 16$). A reasonable consistency in the KAM values at the centre and edge was achieved after HPT for $N = 10$ turns as shown in Figure 4(a). Moreover, as shown also in Figure 4(a), the normalised KAM value of the $N = ½$ turn sample increases from the centre ($\varepsilon_{eq} = 0.8$) to the edge ($\varepsilon_{eq} = 8$) of the disc.

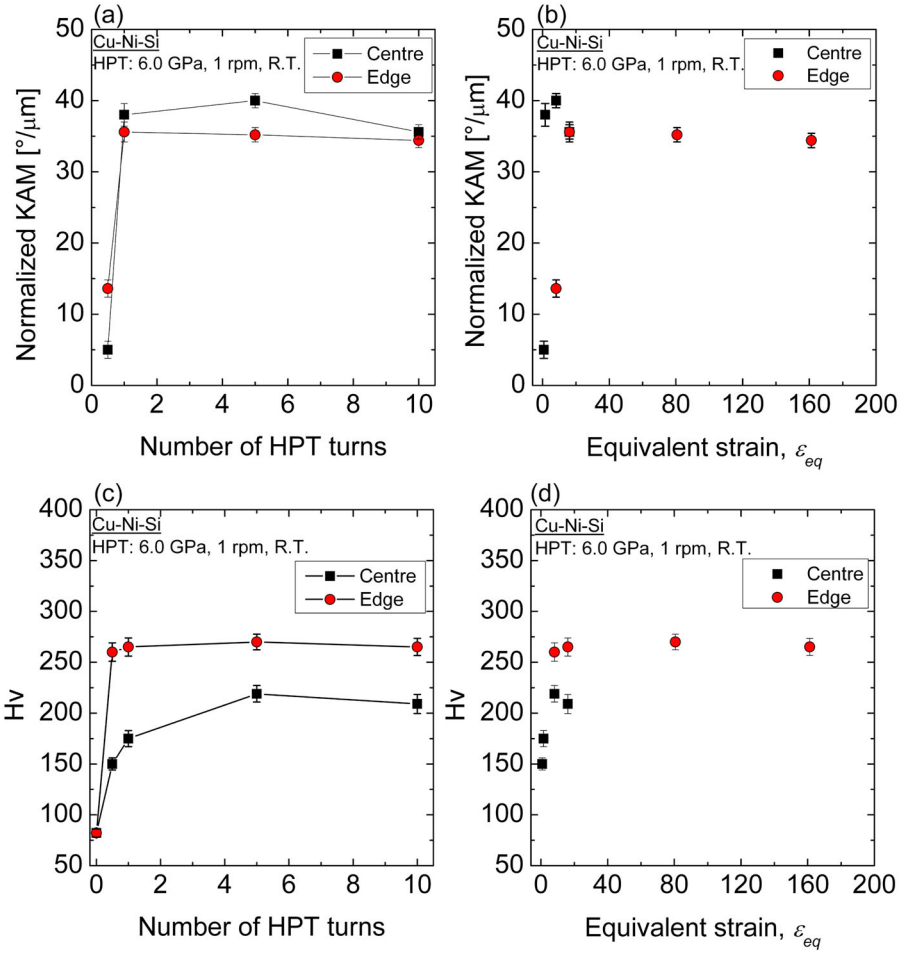

Figure 4. (a, b) Evolution of averaged KAM values as function of number of HPT turns and equivalent strain and (b, c) evolution of mean value of microhardness as function of number of HPT turns and equivalent strain for Cu–Ni–Si alloy processed by HPT for $N = ½$, 1, 5 and 10 turns, respectively.

The evolution of normalised KAM values as a function of equivalent strain is shown in Figure 4(b) for the centres and edges of the Cu–Ni–Si alloy discs after HPT through 10 turns. It is expected that the KAM value continuously increases with increasing strain but instead there is a consistent trend, at both the centres and edges of the Cu–Ni–Si alloy, that the KAM value initially increases dramatically to an equivalent strain of $\varepsilon_{eq} \sim 8$ ($N = ½$ turn) and then it saturates thereafter to a strain of $\varepsilon_{eq} \sim 160$ ($N = 10$ turns). In practice, the KAM value near the edge is lower than the centre after $N = 1$ and $N = 5$ turns but there are similar values after $N = 10$ turns. This indicates that the edges of the processed discs have a smaller internal strain than near the centres of the processed discs.

Figure 4(c,d) show the evolution of microhardness as a function of the numbers of HPT turns and the equivalent strain near the centres and edges of the Cu–Ni–Si alloy discs processed by HPT through $N = ½$, 1, 5 and 10 turns, respectively. It is apparent that the microhardness values at the edges of the processed discs are always much higher than near the centres of the discs, thereby implying an inhomogeneity in the grain size across the disc after HPT for $N = 10$ turns. Moreover, it is expected that the presence of the impurities and the Ni and Si alloying elements in the Cu–Ni–Si alloy contributed to the strain hardening as solid-solution hardening. Actually, it was demonstrated that 15% of the total hardening is due to solid-solution hardening in single-phase alloys processed by HPT [47]. In practice, the microhardness shows saturation around Hv ≈ 260 and reaches a steady-state at the disc edge after $N = ½$ turn ($\varepsilon_{eq} = 8$) while the saturation of Hv ≈ 220 was achieved at the disc centres after $N = 5$ turns ($\varepsilon_{eq} = 8$).

Nevertheless, when the hardness evolution is plotted against equivalent strain as in Figure 4(d) the hardness development at both the centres and the edges of the Cu–Ni–Si alloy tend to show reasonable agreement with the general model for hardening without any microstructural recovery [48]. A large hardness variation without achieving a hardness homogeneity was already reported in pure Cu (99.95 wt.%) and in a Cu–Ag alloy after HPT processing at room temperature for $N = 20$–25 turns [49,50].

Figure 5 presents the evolution of the mean hardness values taken from the Hv values at the disc centre and at the edge for each HPT-processed disc and re-plotted as a function of the inverse of the square root of the mean grain size reported previously [5]. In addition, the data of the same Cu–Ni–Si alloy processed by ECAP at 150°C through $N = 2$, 8 and 12 passes using route A [6] are also plotted to verify the validity of the Hall–Petch relationship over the range of grain sizes produced by HPT and ECAP processing.

These data were fitted using a Hall-Petch equation in the following form in order to examine the contribution of the grain boundary strengthening mechanism to the increase of microhardness as shown in Figure 5 [51]:

$$H_v = H_{v0} + K_H d^{-1/2} \tag{7}$$

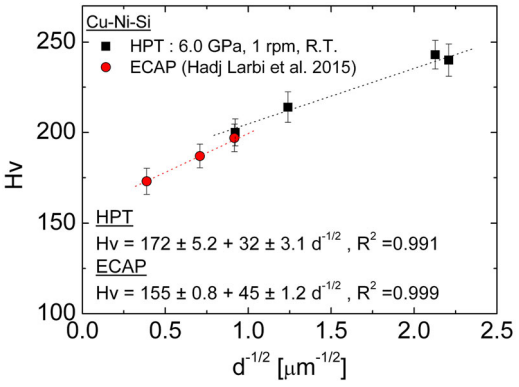

Figure 5. Evolution of microhardness for Cu–Ni–Si alloy processed by HPT for $N = ½$, 1, 5 and 10 turns as function of inverse of the square root of the mean grain size representing the Hall–Petch relationship. Data from the same Cu–Ni–Si alloy processed by ECAP at 150°C through $N = 2$, 8 and 12 passes using route A [6] are also presented.

where H_{v0} is the friction hardness which represents the resistance of the crystal lattice to the movement of dislocations and K_H is a locking parameter which indicates the contribution of the grain boundaries to the hardening.

It is evident from Figure 5 that there is no linear relationship between the microhardness Hv and $d^{-1/2}$ for both the HPT and ECAP-processed Cu–Ni–Si alloy. In this case, the data were treated separately from each type of SPD processing. The linear fit of the datum points gives estimates of $Hv_0 = 172 \pm 5.2$ Hv and $K_H = 32 \pm 3.1$ Hv $\mu m^{1/2}$ with a residual sum $R^2 = 0.991$ for samples processed by HPT and $Hv_0 = 155 \pm 0.8$ Hv, $K_H = 45 \pm 1.2$ Hv $\mu m^{1/2}$ and $R^2 = 0.999$ for samples processed by ECAP.

The difference between the ECAP and HPT processing is a consequence of the much higher strains that can be attained by HPT and this means the grain sizes are generally smaller as may be seen in Figure 5. The present results demonstrate that the Hall–Petch relationship is valid for the Cu–Ni–Si alloy over the range of grain sizes produced by both HPT and ECAP processing.

Figure 6 presents the evolution of stored energy at the disc centres and edges estimated from the DSC method, KAM using Equation (3) and microhardness using Equation (5) plotted as a function of (a) the numbers of HPT turns and (b) the equivalent strain for the Cu–Ni–Si alloy after HPT processing. It is readily apparent from these plots that the stored energy E_{KAM} estimated from KAM increases with increasing numbers of HPT turns to $N = 1$ turn ($\varepsilon_{eq} \sim 16$) and then tends to saturate at ~38 J/mol for both the centres and edges of the processed discs at higher numbers of HPT turns up to $N = 10$ turns ($\varepsilon_{eq} \sim 160$). The stored energy estimated by Hv measurements near the edges is much higher than near the centres of the discs, especially in the early stages of deformation for $N = ½$ ($\varepsilon_{eq} \sim 8$) and $N = 1$ turn ($\varepsilon_{eq} \sim 16$). The increase of the stored energy, E_{Hv}, with increasing numbers of HPT

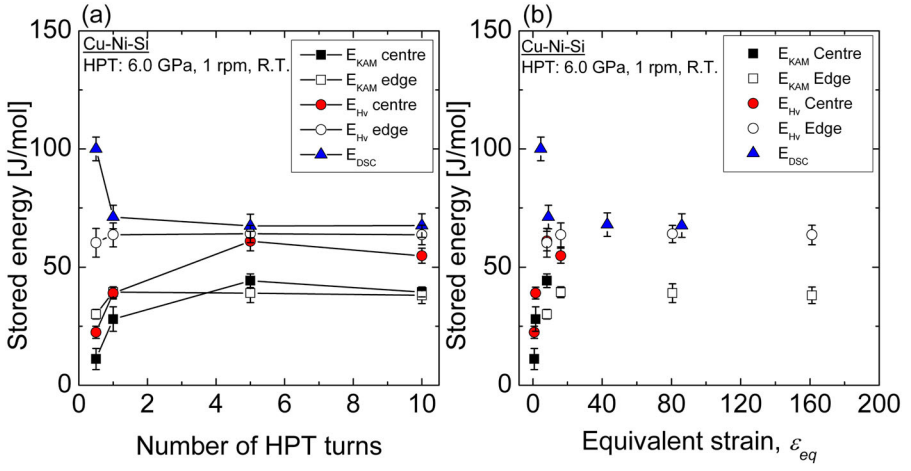

Figure 6. Evolution of stored energy estimated by KAM, Hv and DSC analysis for Cu–Ni–Si alloy processed by HPT for $N = ½$, 1, 5 and 10 turns as function of: (a) number of HPT turns and (b) equivalent strain.

turns is more pronounced near the disc centre where E_{Hv} increases from ~30 J/mol after $N = ½$ turn ($\varepsilon_{eq} \sim 0.8$) to ~ 61 J/mol after $N = 5$ turns ($\varepsilon_{eq} \sim 8$) and then decreases to ~55 J/mol after $N = 10$ turns ($\varepsilon_{eq} \sim 16$). In addition, E_{Hv} at the disc edge after $N = 10$ HPT turns ($\varepsilon_{eq} \sim 160$) reaches $E_{Hv} \approx 60$ J/mol immediately after $N = ½$ turn ($\varepsilon_{eq} \sim 8$) and then slowly increases to ~64 J/mol through $N = 10$ turns ($\varepsilon_{eq} \sim 160$).

It can be recognised from Figure 6 that E_{KAM} at both positions of the disc after $N = ½$ HPT turn were close or even higher than the E_{Hv} at the disc centre after $N = ½$ HPT turn. This is attributed in part to the difference in the step size during the EBSD measurement of the ½ turn disc compared to the other samples as mentioned earlier in the experimental section.

By contrast, the stored energy, E_{DSC}, obtained by the DSC measurements shows a different tendency from these other two approaches where the E_{DSC} value decreases rapidly from ~100 J/mol after $N = ½$ turn ($\varepsilon_{eq} \sim 4.5$) to ~71 J/mol after $N = 1$ turn ($\varepsilon_{eq} \sim 9$) and then exhibits a reasonable saturation at ~67–70 J/mol through $N = 10$ turns ($\varepsilon_{eq} \sim 86$).

It is important to note that the stored energy varies in the following order: $E_{DSC} > E_{Hv} > E_{KAM}$ for all sample conditions. The difference in the estimated stored energy values is attributed directly to the different types of measurements. It is well known that the DSC analysis is used to calculate the energy stored in the vacancies and the different types of dislocations such as geometrically necessary dislocations (GNDs) and statistically stored dislocations (SSDs) [12]. The stored energy estimated via microhardness tests incorporates the contributions of both the GNDs and the SSDs simultaneously [13]. By contrast, the KAM approach is used only to evaluate the stored energy from the GNDs [52,53].

3.2. Activation energy for recrystallization

Considering Equation (6), the plot of $\ln(V/T_p)$ versus $(1000/T_p)$ was constructed as shown in Figure 7(a) by applying the recrystallization peaks measured by the DSC scans at the four heating rates of 10°C/min, 20°C/min, 30°C/min and 40°C/min. It is evident that this Boswell plot shows relative straight lines and the activation energy may be determined directly from the slope of the lines.

Figure 7(b) shows the variation of the estimated activation energy for recrystallization as a function of the equivalent strain for the Cu–Ni–Si alloy. The activation energy increases from 89.7 kJ/mol at $\varepsilon_{eq} \sim 4.5$ ($N = ½$ turn) to 91.8 kJ/mol at $\varepsilon_{eq} \sim 9$ ($N = 1$ turn) and then it slightly increases to ~92.2 kJ/mol through $N =$ 10 turns ($\varepsilon_{eq} \sim 100$). The evolution of the activation energy is in good agreement with the variation of the total stored energy (Figure 6). It is interesting to note that the present range of activation energy (89.7–92.2 kJ/mol) is smaller than the reported activation enthalpy of boundary migration in Cu (106.1 kJ/mol) [54].

4. Discussion

4.1. Significance of the stored energy

The plastic deformation of polycrystalline materials leads to the introduction of different lattice defects such as vacancies and dislocations. These dislocations are classified into GNDs and SSDs. The GNDs accommodate the lattice curvature from the deformation gradient to ensure compatibility requirements which will create orientation gradients in the crystal lattice. The SSDs accumulate due to statistical entanglements and they are formed due to the trapping process of dipoles and/or multipole dislocations [55–57].

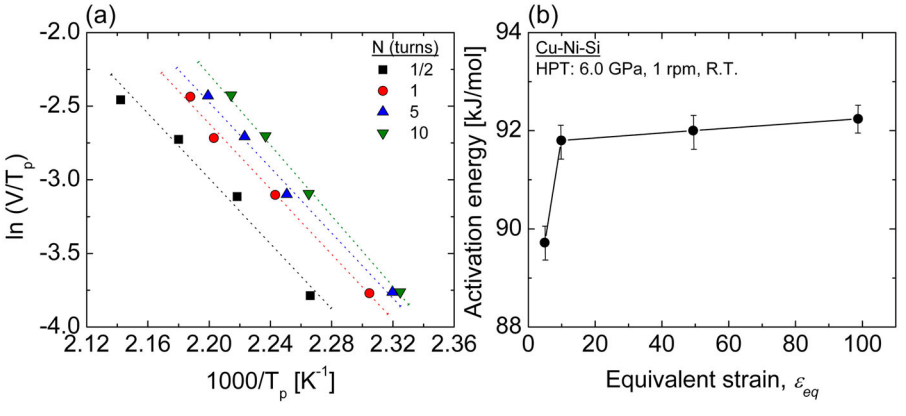

Figure 7. (a) Boswell plots for recrystallization peak in Cu–Ni–Si alloy processed by HPT for $N = ½$, 1, 5 and 10 turns and (b) Evolution of activation energy of recrystallization as function of equivalent strain.

A significant amount of the accumulated energy during plastic deformation is dissipated as heat and the remainder is stored in SSDs, GNDs and vacancies [54]. It is expected that the stored energy will increase with increasing strain. However, the total stored energy estimated by DSC analysis, as shown in Figure 6, decreases in the very early stage of HPT from $N = ½$ to 1 turn ($\varepsilon_{eq} \sim 4.5$) and this implies that the density of defects decreases due to the occurrence of recovery or dynamic recrystallization during processing [25]. The present result shows a saturation of the stored energy and this agrees with several earlier reports on ultrafine-grained oxygen-free high conductivity (OFHC) copper and single phase Cu–Ni–Si and Cu–Cr–Zr alloys [10,18,19] while a decrease in the stored energy was also reported in various FCC alloys after SPD processing [9,21,58]. Furthermore, the recovery rate is faster for HPT copper deformed samples than for ECAP samples [9]. Nevertheless, the stored energy values estimated in the present experiments after HPT processing are even higher than those reported in pure copper processed by ECAP [21].

The stored energy in GNDs measured by the KAM approach in Figure 6(b) achieves a saturation at an equivalent strain of $\varepsilon_{eq} \sim 20$. Such evolution involving the density of GNDs can be explained by the mechanism responsible for grain refinement during HPT processing which has a correlation with the continuous dynamic recrystallization [25]. During the early stage of plastic deformation, dislocation slip systems are activated in different regions of the grains leading to the formation of GNDs to maintain a strain compatibility [59] and this causes a rapid increase in the value of the stored energy. Such rearrangements contribute to the formation of low-angle substructures of cells and sub-grains [59,60] and it is also possible that the heat generated during the deformation contributes to the re-arrangement of dislocations into low-angle grain boundaries (LAGBs) with misorientations lower than 15°. A further increase in deformation straining causes the increase of the misorientation between the cells which leads to the transformation of LAGBs into high-angle grain boundaries (HAGBs, with misorientations higher than 15°) [61] and this leads to the formation of new ultrafine equiaxed grains accompanied by a saturation in the GND density. The GOS maps shown in Figure 3 demonstrate clearly that dynamic recrystallization took place rapidly at an equivalent strain of $\varepsilon_{eq} \sim 8$. Previously, it was shown that the fractions of HAGBs for the present HPT-processed Cu–Ni–Si alloy increase with increasing strain to reach steady state around 65% at an equivalent strain of $\varepsilon_{eq} \sim 80$ [5]. A higher fraction of HAGBs (80%) was found in pure OFHC copper processed by HPT at an equivalent strain of $\varepsilon_{eq} \sim 32$ [25]. This difference is attributed to the delaying effect of the solute atoms (Ni and Si) on the dislocation motion by increasing the localised stress needed for dislocation motion and thereby reducing the amount of LAGBs transformed to HAGBs [47].

It should be noted that the heat generated during HPT processing is in practice very limited and a recent report showed a very small increase in temperature

for several different metals in the very early stages of HPT after processing for <1 turn [62]. Using the general relationship for the prediction of the temperature rise, ΔT, in the sample during HPT processing [63]:

$$\Delta T = 0.22\sigma\omega[1 + 1.28(1 - e^{-(t/482)})] \quad (8)$$

where σ is the stress level, ω is the rotating speed and t is the time for the experimental HPT processing, it was estimated that there was a temperature rise of about $\Delta T = 12$ K after 1 turn and about $\Delta T = 30$ K after 10 turns in the present alloy. A similar value for the temperature rise (~40 K) was reported in pure Cu after $N = 10$ turns using the same experimental conditions [64].

Furthermore, the stored energy in the GNDs is lower at the disc edges by comparison with the centres of the processed discs (Figures 3 and 7) and this is contrary to the distribution of the equivalent strain across the disc radius given in Equation (1). It was demonstrated by scanning electron microscopy that the strain occurs initially at the edge of the discs and with increasing numbers of HPT turns the deformation spreads towards the centre [65]. The high accumulated strain in the edge region leads to the rapid occurrence of dynamic recrystallization and fast softening by comparison with the centre zone where there is a low imposed strain [66,67]. This result is in good agreement with the estimated fraction of recrystallized grains in the present alloy as shown in Figure 3. The dynamic recrystallization is more pronounced at the edges of the discs during the early stage of deformation ($\varepsilon_{eq} \sim 8$–16). With increasing strain in the range of $\varepsilon_{eq} \sim 80$–160 the dynamic recrystallization increases and appears to be more homogenous along the radial distances from the centres of the discs.

The stored energy in SSDs at the centres and edges of the processed discs was estimated from the difference between the stored energy calculated using the microhardness values and the KAM approach and these data are presented in Table 1. The density of SSDs near the centres of the processed discs acts differently to the GNDs where the SSDs increase gradually to ~16.7 J/mol with increasing strain up to $N = 5$ turns ($\varepsilon_{eq} = 8$) and decreases slightly to ~15.4 J/mol after $N = 10$ turns ($\varepsilon_{eq} = 16$). By contrast, the magnitude of the stored energy in SSDs near the edge of the processed discs is high after $N = ½$ turn

Table 1. Estimation of stored energy of SSDs dislocations ($E_{Hv} - E_{KAM}$) and vacancies ($E_{DSC} - E_{Hv}$) as function of the number of HPT turns. True dislocation density (ρ_{XRD}) estimated using XRDLPA [8], corresponding stored energy (E_{XRD}) and stored energy of vacancies ($E_{vac'} = E_{DSC} - E_{XRD}$).

	E_{SSD} (J/mol) (E_{DSC}–E_{Hv})		E_{vac} (J/mol) (E_{DSC}–E_{Hv})	ρ_{XRD} (× 10^{15} m^{-2})	E_{XRD} (J/mol)	$E_{vac'}$ (J/mol) (E_{DSC}–E_{XRD})
N	centre	edge				
½	11.3	30.2	58.6	4.93	42.23	57.76
1	11.0	24.2	19.8	7.29	59.41	11.68
5	16.7	26.0	4.3	7.58	61.45	6.44
10	15.4	25.5	8.2	7.59	61.52	5.97

($\varepsilon_{eq} = 8$) and then decreases to ~24.2 J/mol after $N = 1$ turn ($\varepsilon_{eq} = 16$) and appears to stabilise with increasing numbers of HPT turns up to $N = 10$ turns ($\varepsilon_{eq} = 160$).

It was reported that the GND density was 3 times higher than the SSD density in HPT-processed copper annealed at a low temperature of 100°C [26]. Studies found that only 3.5% of the total stored energy was from the SSD and 44% from the contribution of GND in OFHC copper processed by ECAP through 8 passes using route *Bc* [10]. In addition, it was reported that 10% from the stored energy estimated by neutron diffraction (taking into account both SSD and GND) is attributed to the SSD in strongly cold rolled Fe-48Ni (wt.%) alloy [37]. In the present study, the GND density exceeds the SSD density only near the centre of the processed discs and in the early stage of deformation $\varepsilon_{eq} \sim 0.8$–$1.6$ (N = ½ and 1 turn) but with a further increase of strain to $\varepsilon_{eq} \sim 16$ ($N = 5$ turns) the contribution to the stored energy was similar. It is reasonable to conclude that this similarity is due to a balance between the rates of dislocation nucleation and recovery.

The stored energy of the vacancies is summarised in Table 1 which was estimated from the difference between the stored energy of DSC and the Hv measurements. It should be noted that the mean value corresponding to the centre and the edge of the discs was used to obtain the mean stored energy from the Hv measurements. As can be seen from these data, an increase in numbers of HPT turns leads to a decrease in their concentration. Since the dislocation density decreases with increasing strain near the edges of the discs, it is reasonable to assume a similar decrease for vacancies. However, it can be observed that the stored energy of vacancies (58.6 J/mol) exceeds that for dislocations ($E_{Hv} \sim 41.3$ J/mol) in the early stage of deformation (N = ½ HPT turn). In fact, several studies demonstrated that SPD processing leads to the development of a very high concentration of vacancies [14,50].

For comparison, the dislocation density estimated previously for the same Cu–Ni–Si samples by an X-ray diffraction line profile analysis (XRDLPA) [8] was used to calculate their stored energy using the following equation based on DSC measurements [68]:

$$E_{XRD} = \mu b^2 \frac{\rho_{XRD}}{4\pi\epsilon} \ln\left(\frac{1}{b\sqrt{\rho_{XRD}}}\right) \tag{9}$$

where ρ_{XRD} is the dislocation density, ε is the arithmetic average of 1 and $(1-\upsilon)$ and υ is the Poisson ratio ($\upsilon = 0.355$) for copper.

It is reasonably assumed that the dislocation density estimated by XRDLPA represents the true dislocation density [69] present in the deformed materials since XRDLPA is able to quantify the lattice distortions caused by defects that are larger than 5 nm [70]. Therefore, it can be considered that the dislocation density estimation from XRDLPA involved both SSD and GND [71].

In this case, the stored energy from the vacancies $E_{vac'}$ was calculated from the difference between E_{DSC} and E_{XRD}. In fact, the correlation between the DSC analysis and the XRDLPA approach is a procedure often used to estimate the concentration of vacancies in severely deformed materials [14,69,72–74]. The evolution of ρ_{XRD}, E_{XRD} and $E_{vac'}$ as a function of the number of HPT turns are summarised in Table 1. It can be clearly seen that the values of the stored energy of the vacancies ($E_{vac} = E_{DSC} - E_{XRD}$) are very close to those calculated from the difference ($E_{vac} = E_{DSC} - E_{Hv}$). It may be concluded that the use of the Hv procedure gives a good estimation of the sorted energy of both dislocation types (SSD and GND).

The concentration of vacancies may be estimated based on the stored energy using the following equation:

$$C_v = \frac{E_{vac}}{86.84.10^3} \tag{10}$$

where 86.84×10^3 J/mol $\approx$ 0.9 eV is the vacancy formation energy in copper [75].

Thus, the concentration of vacancies is estimated as in the range of ~1.0–6.7×10^{-4} where these values are in the same range as those reported in copper processed by ECAP [14] and they are much higher than in copper deformed by conventional deformation such as cold rolling [14,72]. In practice, it was demonstrated that the variation of the vacancy concentration is more sensitive to the extent of hydrostatic pressure than the dislocation density [14]. This is consistent with the present results where a high concentration of vacancies is produced after $N = ½$ turn and the significant decrease in the vacancy concentration after $N = 5$ turns is attributed to the role of vacancies in the climb of dislocations during processing [72]. In severely deformed copper the vacancies are generated as agglomerates and no single or double vacancies were observed due to the medium value of the stacking fault energy [72].

The creation and annihilation of vacancies play an important role in the hardening of materials during deformation [76]. Thus, the presence of a high concentration of vacancies can retard the movement of dislocations leading to an increase in the strength of the material.

It may be concluded that, in the initial stage of deformation at $\varepsilon_{eq} \sim 0.8$–1.6 ($N = ½$–1 turn), the high densities of dislocations are mostly of the GND type and vacancies are produced in order to accommodate grain rotation and the formation of an ultrafine microstructure. With further increase in the numbers of HPT turns, and after the formation of the fine microstructure, the dislocations are in SDD type and play an important role in accommodating the deformation process. This conclusion is consistent with the TEM observations which demonstrate that a high dislocation density is present at sub-grain boundaries during the early stage of the HPT process and these dislocations were not visible within each sub-grain [60,77]. By contrast, at high deformation strains the

dislocations are observed within the grains and this corresponds to the SSD dislocations [77].

4.2. Significance of the activation energy

The activation energy of recrystallization calculated in the present Cu–Ni–Si alloy was in the range of ¬89.7–92.2 kJ/mol, depending on the imposed strain. It was found that the activation energy increases rapidly at low equivalent strain ($\varepsilon_{eq} \sim 10$) and more slowly at higher equivalent stain ($\varepsilon_{eq} \sim 50$). However, some studies demonstrated that the activation energy of recrystallization decreases with increasing strain in severely deformed copper-based alloys [10,19,78]. Such evolution was explained by the excessive formation of vacancy agglomerates with increasing strain [10]. Table 1 shows that the vacancy concentration decreases drastically soon after $N = ½$ turn due to the dynamic recrystallization which probably explains the increase of the activation energy of recrystallization with further strain increases. Moreover, the annihilation of the dislocations needs more activation enthalpy due to their rearrangement at high strains [78].

A compilation of different values for the activation energy of variously deformed copper-based alloys is listed in Table 2. The present values of the activation energy are somewhat lower than those found for the same alloy processed by ECAP via route A up to 12 passes at 150°C [18]. This may be explained by the higher strain introduced in the material by HPT relative to processing by ECAP. Table 2 shows that copper-based alloys processed by ECAP have a high activation energy compared to HPT processing. These results demonstrate that the HPT processing exhibits poor thermal stability compared to ECAP processing. However, a lower activation energy of ~65 kJ/mol was calculated from hardness tests of a copper alloy after 12 ECAP passes [17]. Moreover, it appears that the activation energy varies significantly with the elemental additions in the alloys. For example, the addition of only 0.0068 at.% of copper to pure aluminum raised the activation energy for recrystallization from ~60 to ~120 kJ/mol [54].

Table 2. Activation energy values of recrystallization process of various copper alloys compiled from the literature.

Material	Processing condition	Activation energy (kJ/mol)	References
Pure copper	ECAP	99–65	[18]
Pure copper	ECAP	91–99	[11]
Pure copper	ECAP	117–121	[4]
Pure copper	ECAP	62–111	[79]
Pure copper	HPT	94	[27]
Cu–Ni–Si	ECAP	127	[17]
Cu–Cr–Zr	ECAP	117–135	[19]
Oxygen-free high conductivity (OFHC) copper	ECAP	80	[10]
Pure copper	Cold rolling	104	[80]
Pure copper	Cold rolling	108	[18]

It was assumed that the activation energy of recrystallization is independent of the stored energy in ECAP-processed high purity copper and at high strains the recrystallization kinetics are more dependent on structural factors such as the grain size rather than on the stored energy [21]. However, the evolution of activation energy of recrystallization in the present Cu–Ni–Si alloy demonstrates a net dependency on the stored energy. As expected, the activation energy of the recrystallization increases with decreasing stored energy in the alloy. In fact, the decrease in the stored energy due to the occurrence of dynamic recrystallization causes a decrease of the driving force for recrystallization and thereby an increase in the activation energy.

Thus, the evolution of the total stored energy and local stored energy in GNDs, SSDs and vacancies was estimated during increasing strain in the HPT processing and as a function of the radial distances from the centres of the discs. Further, the evolution activation energy of the recrystallization was also calculated as a function of the number of HPT turns. The present results contribute towards our understanding of the recrystallization mechanism in severely deformed materials.

Conclusions

1. A commercial Cu–Ni–Si alloy was subjected to HPT processing at room temperature up to 10 turns and the stored energy and activation energy for recrystallization were estimated using differential scanning calorimetry, electron backscatter diffraction and Vickers microhardness.
2. The fraction of recrystallized grains increases rapidly to 25% at the edge of the $N = ½$ turn disc ($\varepsilon_{eq} = 8$). The microstructure was more homogenised along the radial distance of the disc processed through $N = 10$ turns ($\varepsilon_{eq} = 160$) and contained about 30–35% of recrystallized grains in both the disc centre and edge.
3. The Hall–Petch relationship is valid for the Cu–Ni–Si alloy over the range of grain sizes produced by HPT and ECAP processing.
4. The total stored energy calculated from DSC measurements decreases rapidly after $\varepsilon_{eq} = 16$ ($N = 1$ turn) but then stabilises at ~70 J/mol for processing up to $\varepsilon_{eq} = 86$ ($N = 10$ HPT turns). This decrease is attributed to the rapid occurrence of dynamic recrystallization during the earlier stage of HPT processing. The local stored energy estimated from the KAM approach (GNDs) and Hv (GNDs + SSDs) measurements was shown to be inhomogeneous along the radial distance from the centre of the HPT-processed disc and increased with increasing equivalent strain at $\varepsilon_{eq} \sim 16$ and saturated with further strain increases.
5. GNDs and vacancies are responsible for the high stored energy in the initial stage of deformation at $\varepsilon_{eq} = 8.6$–16 ($N = ½$–1 turn). The contribution of the

SSDs is similar to that of the GNDs only in high strain deformation as at ε_{eq} = 49.3 (N = 5 turns) when dynamic recrystallization is occurring.

6. The recrystallization temperature was in the range of 157–194°C. It increases with increasing heating rate and decreases with increasing numbers of HPT turns. A low value in the range of ~ 89.7–98.7 kJ/mol was measured for the activation energy of recrystallization, thereby suggesting a poor thermal stability.

Acknowledgements

The authors wish to thank Mr. Hacen Hadj Larbi from CLAL-FRANCE for kindly providing the Cu–Ni–Si alloy. One of the authors (YIB) wishes to heartily thank Prof. Jose Maria Cabrera from Polytecnia ETSEIB, Universidad Politécnica de Cataluña (UPC), for an invitation to UPC and for help during the scientific research and to the staff of the Biomaterials research group of UPC for their support in the DSC analysis.

Disclosure statement

No potential conflict of interest was reported by the authors.

Funding

This study was supported in part by the National Science Foundation of the United States under Grant No. DMR-1810343 (MK) and in part by the European Research Council under ERC Grant Agreement No. 267464-SPDMETALS (TGL).

ORCID

Megumi Kawasaki http://orcid.org/0000-0003-0028-3007
Terence G. Langdon https://orcid.org/0000-0003-3541-9250

References

[1] R.Z. Valiev and T.G. Langdon, *Principles of equal-channel angular pressing as a processing tool for grain refinement*, Prog. Mater. Sci. 51 (2006), pp. 881–981.
[2] A.P. Zhilyaev and T.G. Langdon, *Using high-pressure torsion for metal processing: Fundamentals and applications*, Prog. Mater. Sci. 53 (2008), pp. 893–979.
[3] F. Dalla Torre, R. Lapovok, J. Sandlin, P.F. Thomson, C.H.J. Davies, and E.V. Pereloma, *Microstructures and properties of copper processed by equal channel angular extrusion for 1–16 passes*, Acta Mater. 52 (2004), pp. 4819–4832.
[4] N. Lugo, N. Llorca, J.J. Suñol, and J.M. Cabrera, *Thermal stability of ultrafine grains size of pure copper obtained by equal-channel angular pressing*, J. Mater. Sci. 45 (2010), pp. 2264–2273.
[5] A.Y. Khereddine, F. Hadj Larbi, H. Azzeddine, T. Baudin, F. Brisset, A.-L. Helbert, M.-H. Mathon, M. Kawasaki, D. Bradai, and T.G. Langdon, *Microstructures and textures of*

a Cu–Ni–Si alloy processed by high-pressure torsion, J. Alloys Compd. 574 (2013), pp. 361–367.

[6] F. Hadj Larbi, H. Azzeddine, T. Baudin, M.-H. Mathon, F. Brisset, A.-L. Helbert, M. Kawasaki, D. Bradai, and T.G. Langdon, *Microstructure and texture evolution in a Cu–Ni–Si alloy processed by equal-channel angular pressing*, J. Alloys Compd. 638 (2015), pp. 88–94.

[7] K. Abib, J.A.M. Balanos, B. Alili, and D. Bradai, *On the microstructure and texture of Cu-Cr-Zr alloy after severe plastic deformation by ECAP*, Mater. Charact. 112 (2016), pp. 252–258.

[8] A.Y. Khereddine, F.H. Larbi, M. Kawasaki, T. Baudin, D. Bradai, and T.G. Langdon, *An examination of microstructural evolution in a Cu–Ni–Si alloy processed by HPT and ECAP*, Mater. Sci. Eng. A. 576 (2013), pp. 149–155.

[9] M.Y. Alawadhi, S. Sabbaghianrad, Y. Huang, and T.G. Langdon, *Direct influence of recovery behaviour on mechanical properties in oxygen-free copper processed using different SPD techniques: HPT and ECAP*, J. Mater. Res. Technol. 6 (2017), pp. 369–377.

[10] W.Q. Cao, C.F. Gu, E.V. Pereloma, and C.H.J. Davies, *Stored energy, vacancies and thermal stability of ultra-fine grained copper*, Mater. Sci. Eng. A. 492 (2008), pp. 74–79.

[11] Y.L. Wang, R. Lapovok, J.T. Wang, Y.S. Qi, and Y. Estrin, *Thermal behavior of copper processed by ECAP with and without back pressure*, Mater. Sci. Eng. A. 628 (2015), pp. 21–29.

[12] N. Gao, M.J. Starink, and T.G. Langdon, *Using differential scanning calorimetry as an analytical tool for ultrafine grained metals processed by severe plastic deformation*, Mater. Sci. Technol. 25 (2009), pp. 687–698.

[13] S.S. Hazra, A.A. Gazder, and E.V. Pereloma, *Stored energy of a severely deformed interstitial free steel*, Mater. Sci. Eng. A. 524 (2009), pp. 158–167.

[14] E. Schafler, G. Steiner, E. Korznikova, M. Kerber, and M.J. Zehetbauer, *Lattice defect investigation of ECAP-Cu by means of X-ray line profile analysis, calorimetry and electrical resistometry*, Mater. Sci. Eng. A. 410-411 (2005), pp. 169–173.

[15] A.L. Etter, T. Baudin, M.H. Mathon, W. Swiatnicki, and R. Penelle, *Stored energy evolution in both phases of a duplex steel as a function of cold rolling reduction*, Scr. Mater. 54 (2006), pp. 683–688.

[16] C. Fressengeas, B. Beausir, C. Kerisit, A.-L. Helbert, T. Baudin, F. Brisset, M.-H. Mathon, R. Besnard, and N. Bozzolo, *On the evaluation of dislocation densities in pure tantalum from EBSD orientation data*, Matér. Tech. 106 (2018), p. 604.

[17] X. Molodova, G. Gottstein, M. Winning, and R.J. Hellmig, *Thermal stability of ECAP processed pure copper*, Mater. Sci. Eng. A. 460-461 (2007), pp. 204–213.

[18] F. Hadj-Larbi, K. Abib, A.E.Y. Khereddine, B. Alili, M. Kawasaki, D. Bradai, and T.G. Langdon, *DSC analysis of an ecapdeformed Cu-Ni-Si alloy*, Proceedings 22 International Conference on Metallurgy and Materials (Metal'2013), Brno, Czech Republic, 2013.

[19] K. Abib, F.H. Larbi, L. Rabahi, B. Alili, and D. Bradai, *DSC Analysis of Commercial Cu–Cr–Zr Alloy Processed by Equal Channel Angular Pressing*, Trans. Nonferr. Met. Soc. China. 25 (2015), pp. 838–843.

[20] K. Abib, H. Azzeddine, K. Tirsatine, T. Baudin, A.-L. Helbert, F. Brisset, B. Alili, and D. Bradai, *Thermal stability of Cu-Cr-Zr alloy processed by equal-channel angular pressing*, Mater. Charact. 118 (2016), pp. 527–534.

[21] Y. Zhang, J.T. Wang, C. Cheng, and J. Liu, *Stored energy and recrystallization temperature in high purity copper after equal channel angular pressing*, J. Mater. Sci. 43 (2008), pp. 7326–7330.

[22] A.P. Zhilyaev, I. Shakhova, A. Belyakov, R. Kaibyshev, and T.G. Langdon, *Effect of annealing on wear resistance and electroconductivity of copper processed by high-pressure torsion*, J. Mater. Sci. 49 (2014), pp. 2270–2278.
[23] Z. Horita and T.G. Langdon, *Microstructures and microhardness of an aluminum alloy and pure copper after processing by high-pressure torsion*, Mater. Sci. Eng. A. 410-411 (2005), pp. 422–425.
[24] E. Schafler and M.B. Kerber, *Microstructural investigation of the annealing behaviour of high-pressure torsion (HPT) deformed copper*, Mater. Sci. Eng. A. 462 (2007), pp. 139–143.
[25] A. Vorhauer, S. Scheriau, and R. Pippan, *In-situ annealing of severe plastic-deformed OFHC copper*, Metall. Mater. Trans. A. 39 (2008), pp. 908–918.
[26] A.P. Zhilyaev, S.N. Sergeev, and T.G. Langdon, *Electron backscatter diffraction (EBSD) microstructure evolution in HPT copper annealed at a low temperature*, J. Mater. Res. Technol. 3 (2014), pp. 338–343.
[27] H. Jiang, Y.T. Zhu, D.P. Butt, I.V. Alexandrov, and T.C. Lowe, *Microstructural evolution, microhardness and thermal stability of HPT-processed Cu*, Mater. Sci. Eng. A. 290 (2000), pp. 128–138.
[28] J. Čížek, I. Procházka, M. Cieslar, R. Kužel, Z. Matěj, V. Cherkaska, R.K. Islamgaliev, and O. Kulyasova, *Influence of ceramic nanoparticles on grain growth in ultra fine grained copper prepared by high pressure torsion*, Phys. Status Solidi C. 4 (2007), pp. 3587–3590.
[29] Y. Huang, S. Sabbaghianrad, A.I. Almazrouee, K.J. Al-Fadhalah, S.N. Alhajeri, and T.G. Langdon, *The significance of self-annealing at room temperature in high purity copper processed by high-pressure torsion*, Mater. Sci. Eng. A. 656 (2016), pp. 55–66.
[30] Y. Huang, S. Sabbaghianrad, A.I. Almazrouee, K.J. Al-Fadhalah, S.N. Alhajeri, N.X. Zhang, and T.G. Langdon, *Comparisons of self-annealing behaviour of HPT-processed high purity Cu and a Pb–Sn alloy*, J. Mater. Res. Technol. 6 (2017), pp. 390–395.
[31] A.I. Almazrouee, K.J. Al-Fadhalah, S.N. Alhajeri, Y. Huang, and T.G. Langdon, *Effect of long-term storage on microstructure and microhardness stability in OFHC copper processed by high-pressure torsion*, Adv. Eng. Mater. 21 (2019), p. 1801300.
[32] R.B. Figueiredo, P.R. Cetlin, and T.G. Langdon, *Using finite element modeling to examine the flow processes in quasi-constrained high-pressure torsion*, Mater. Sci. Eng. A. 528 (2011), pp. 8198–8204.
[33] P.H.R. Pereira, R.B. Figueiredo, P.R. Cetlin, and T.G. Langdon, *An examination of the elastic distortions of anvils in high-pressure torsion*, Mater. Sci. Eng. A. 631 (2015), pp. 201–208.
[34] Y. Mikami, K. Oda, M. Kamaya, and M. Mochizuki, *Effect of reference point selection on microscopic stress measurement using EBSD*, Mater. Sci. Eng. A. 647 (2015), pp. 256–264.
[35] J.-H. Cho, A.D. Rollett, and K.H. Oh, *Determination of a mean orientation in electron backscatter diffraction measurements*, Metall. Mater. Trans. A. 36 (2005), pp. 3427–3438.
[36] R. Badji, T. Chauveau, and B. Bacroix, *Texture, misorientation and mechanical anisotropy in a deformed dual phase stainless steel weld joint*, Mater. Sci. Eng. A. 575 (2013), pp. 94–103.
[37] Y. Ateba Betanda, A.-L. Helbert, F. Brisset, M.-H. Mathon, T. Waeckerlé, and T. Baudin, *Measurement of stored energy in Fe–48%Ni alloys strongly cold-rolled using three approaches: Neutron diffraction, Dillamore and KAM approaches*, Mater. Sci. Eng. A. 614 (2014), pp. 193–198.

[38] Q. Liu, D. Juul Jensen, and N. Hansen, *Effect of grain orientation on deformation structure in cold-rolled polycrystalline aluminium*, Acta Mater. 46 (1998), pp. 5819–5838.
[39] Y. Takayama and J.A. Szpunar, *Stored energy and Taylor factor relation in an Al-Mg-Mn alloy sheet worked by continuous cyclic bending*, Mater. Trans. 45 (2004), pp. 2316–2325.
[40] Y. Takayama, J.A. Szpunar, and H. Kato, *Analysis of intragranular misorientation related to deformation in an Al-Mg-Mn alloy*, Mater. Sci. Forum 495-497 (2005), pp. 1049–1054.
[41] S.I. Wright, M.M. Nowell, R. de Kloe, and L. Chan, *Orientation precision of electron backscatter diffraction measurements near grain boundaries*, Microsc. Microanal. 20 (2014), pp. 852–863.
[42] C. Moussa, M. Bernacki, R. Besnard, and N. Bozzolo, *About quantitative EBSD analysis of deformation and recovery substructures in pure Tantalum*, IOP Conf. Ser.: Mater. Sci. Eng. 89 (2015), p. 012038.
[43] G.I. Taylor, *The mechanism of plastic deformation of crystals. part I.-Theoretical*, Proc. R. Soc. Lond. A. 145 (1934), pp. 362–387.
[44] H.E. Kissinger, *Reaction kinetics in differential thermal analysis*, Anal. Chem. 29 (1957), pp. 1702–1706.
[45] P.G. Boswell, *On the calculation of activation energies using a modified Kissinger method*, J. Therm. Anal. 18 (1980), pp. 353–358.
[46] H. Azzeddine, B. Mehdi, L. Hennet, D. Thiaudière, B. Alili, M. Kawasaki, D. Bradai, and T.G. Langdon, *An in situ synchrotron X-ray diffraction study of precipitation kinetics in a severely deformed Cu–Ni–Si alloy*, Mater. Sci. Eng. A. 597 (2014), pp. 288–294.
[47] K. Edalati, D. Akama, A. Nishio, S. Lee, Y. Yonenaga, J.M. Cubero-Sesin, and Z. Horita, *Influence of dislocation–solute atom interactions and stacking fault energy on grain size of single-phase alloys after severe plastic deformation using high-pressure torsion*, Acta Mater. 69 (2014), pp. 68–77.
[48] M. Kawasaki, *Different models of hardness evolution in ultrafine-grained materials processed by high-pressure torsion*, J. Mater. Sci. 49 (2014), pp. 18–34.
[49] Y.Z. Tian, S.D. Wu, Z.F. Zhang, R.B. Figueiredo, N. Gao, and T.G. Langdon, *Microstructural evolution and mechanical properties of a two-phase Cu–Ag alloy processed by high-pressure torsion to ultrahigh strains*, Acta Mater. 59 (2011), pp. 2783–2796.
[50] J. Čížek, M. Janeček, O. Srba, R. Kužel, Z. Barnovská, I. Procházka, and S. Dobatkin, *Evolution of defects in copper deformed by high-pressure torsion*, Acta Mater. 59 (2011), pp. 2322–2329.
[51] R.W. Armstrong, *Engineering science aspects of the Hall–Petch relation*, Acta Mech. 225 (2014), pp. 1013–1028.
[52] W. Pantleon, *Resolving the geometrically necessary dislocation content by conventional electron backscattering diffraction*, Scr. Mater. 58 (2008), pp. 994–997.
[53] D.P. Field, C.C. Merriman, N. Allain-Bonasso, and F. Wagner, *Quantification of dislocation structure heterogeneity in deformed polycrystals by EBSD*, Modell. Simul. Mater. Sci. Eng. 20 (2012), p. 024007.
[54] J. Humphreys, G.S. Rohrer, and A. Rollett, *Chapter 7 – recrystallization of single-phase alloys*, in *Recrystallization and Related Annealing Phenomena*, 3rd ed., J. Humphreys, G.S. Rohrer and A. Rollett, eds., Elsevier, Oxford, 2017, pp. 245–304.
[55] M.F. Ashby, *The deformation of plastically non-homogeneous materials*, Philos. Mag. A.: J. Theor. Exp. Appl. Phys. 21 (1970), pp. 399–424.

[56] J. Jiang, T.B. Britton, and A.J. Wilkinson, *Evolution of dislocation density distributions in copper during tensile deformation*, Acta Mater. 61 (2013), pp. 7227–7239.
[57] P.J. Konijnenberg, S. Zaefferer, and D. Raabe, *Assessment of geometrically necessary dislocation levels derived by 3D EBSD*, Acta Mater. 99 (2015), pp. 402–414.
[58] Y. Murata, I. Nakaya, and M. Morinaga, *Assessment of strain energy by measuring dislocation density in copper and aluminium prepared by ECAP and ARB*, Mater. Trans. 49 (2008), pp. 20–23.
[59] D. Kuhlmann-Wilsdorf, and N. Hansen, *Geometrically necessary, incidental and subgrain boundaries*, Scr. Metall. Mater. 25 (1991), pp. 1557–1562.
[60] A. Belyakov, T. Sakai, H. Miura, and K. Tsuzaki, *Grain refinement in copper under large strain deformation*, Philos. Mag. A. 81 (2001), pp. 2629–2643.
[61] O. Renk, P. Ghosh, and R. Pippan, *Generation of extreme grain aspect ratios in severely deformed tantalum at elevated temperatures*, Scr. Mater. 137 (2017), pp. 60–63.
[62] K. Edalati, Y. Hashiguchi, P.H.R. Pereira, Z. Horita, and T.G. Langdon, *Effect of temperature rise on microstructural evolution during high-pressure torsion*, Mater. Sci. Eng. A. 714 (2018), pp. 167–171.
[63] P.H.R. Pereira, R.B. Figueiredo, Y. Huang, P.R. Cetlin, and T.G. Langdon, *Modeling the temperature rise in high-pressure torsion*, Mater. Sci. Eng. A. 593 (2014), pp. 185–188.
[64] K. Edalati, R. Miresmaeili, Z. Horita, H. Kanayama, and R. Pippan, *Significance of temperature increase in processing by high-pressure torsion*, Mater. Sci. Eng. A. 528 (2011), pp. 7301–7305.
[65] Y.Z. Tian, X.H. An, S.D. Wu, Z.F. Zhang, R.B. Figueiredo, N. Gao, and T.G. Langdon, *Direct observations of microstructural evolution in a two-phase Cu–Ag alloy processed by high-pressure torsion*, Scr. Mater. 63 (2010), pp. 65–68.
[66] C. Xu, Z. Horita, and T.G. Langdon, *The evolution of homogeneity in processing by high-pressure torsion*, Acta Mater. 55 (2007), pp. 203–212.
[67] A. Hanna, H. Azzeddine, R. Lachhab, T. Baudin, A.-L. Helbert, F. Brisset, Y. Huang, D. Bradai, and T.G. Langdon, *Evaluating the textural and mechanical properties of an Mg-Dy alloy processed by high-pressure torsion*, J. Alloys Compd. 778 (2019), pp. 61–71.
[68] M.B. Bever, D.L. Holt, and A.L. Titchener, *The stored energy of cold work*, Prog. Mater. Sci. 17 (1973), pp. 5–177.
[69] T. Ungár, E. Schafler, P. Hanák, S. Bernstorff, and M. Zehetbauer, *Vacancy production during plastic deformation in copper determined by in situ X-ray diffraction*, Mater. Sci. Eng. A. 462 (2007), pp. 398–401.
[70] T. Ungar, H. Mughrabi, D. Rönnpagel, and M. Wilkens, *X-ray line-broadening study of the dislocation cell structure in deformed [001]-orientated copper single crystals*, Acta Metall. 32 (1984), pp. 333–342.
[71] J. Gubicza, I. Schiller, N.Q. Chinh, J. Illy, Z. Horita, and T.G. Langdon, *The effect of severe plastic deformation on precipitation in supersaturated Al–Zn–Mg alloys*, Mater. Sci. Eng. A. 460-461 (2007), pp. 77–85.
[72] D. Setman, E. Schafler, E. Korznikova, and M.J. Zehetbauer, *The presence and nature of vacancy type defects in nanometals detained by severe plastic deformation*, Mater. Sci. Eng. A. 493 (2008), pp. 116–122.
[73] M. El-Tahawy, Y. Huang, T. Um, H. Choe, J.L. Lábár, T.G. Langdon, and J. Gubicza, *Stored energy in ultrafine-grained 316L stainless steel processed by high-pressure torsion*, J. Mater. Res. Technol. 6 (2017), pp. 339–347.
[74] G. Kapoor, L. Péter, É. Fekete, J.L. Lábár, and J. Gubicza, *Stored energy in nanocrystalline Ni-Mo films processed by electrodeposition*, J. Alloys Compd. 796 (2019), pp. 307–313.

[75] C.J. Meechan and R.R. Eggleston, *Formation energies of vacancies in copper and gold*, Acta Metall. 2 (1954), pp. 680–683.
[76] M. Zehetbauer, G. Steiner, E. Schafler, A.V. Korznikov, and E. Korznikova, *Deformation induced vacancies with severe plastic deformation: Measurements and modelling*, Mater. Sci. Forum 503-504 (2006), pp. 57–64.
[77] Y.B. Wang, J.C. Ho, X.Z. Liao, H.Q. Li, S.P. Ringer, and Y.T. Zhu, *Mechanism of grain growth during severe plastic deformation of a nanocrystalline Ni–Fe alloy*, Appl. Phys. Lett. 94 (2009), p. 011908.
[78] D. Setman, M.B. Kerber, E. Schafler, and M.J. Zehetbauer, *Activation enthalpies of deformation-induced lattice defects in severe plastic deformation Nanometals measured by differential scanning calorimetry*, Metall. Mater. Trans. A. 41 (2010), pp. 810–815.
[79] O.F. Higuera-Cobos and J.M. Cabrera, *Mechanical, microstructural and electrical evolution of commercially pure copper processed by equal channel angular extrusion*, Mater. Sci. Eng. A. 571 (2013), pp. 103–114.
[80] H.D. Mengelberg, M. Meixner, and K. Lücke, *Zur kinetik der rekristallisation von kupfer nach tieftemperaturverformung*, Acta Metall. 13 (1965), pp. 835–844.